Available online at www.sciencedirect.com
ScienceDirect
Journal of Magnetic Resonance 185 (2007) 130–137
JMR Journal of Magnetic Resonance
www.elsevier.com/locate/jmr

Imaged deconvolution: A method for extracting high-resolution NMR spectra from inhomogeneous fields

Meghan E. Halse, Paul T. Callaghan *

MacDiarmid Institute for Advanced Materials and Nanotechnology, School of Chemical and Physical Sciences, Victoria University of Wellington, Wellington 6001, New Zealand

Received 9 October 2006; revised 5 December 2006
Available online 28 December 2006

Abstract

We present a novel method for obtaining high resolution NMR spectra in the presence of grossly inhomogeneous magnetic fields, such as those encountered in one-sided access NMR. Our method combines the well-known principle of reference deconvolution with NMR imaging in order to resolve spectral features with frequency resolution orders of magnitude smaller than the prevailing line-broadening due to field inhomogeneity. We demonstrate that, in cases of inhomogeneous field line-broadening more than an order of magnitude larger than the spectral features to be resolved, rather than performing reference deconvolution on the sample as a whole, it is more favourable in terms of SNR to divide the target region of a sample into smaller sub-regions, by means of chemical shift imaging, and then to perform reference deconvolution on the individual sub-region spectra, finally summing the results In this way, significant resolution enhancements can be obtained in the presence of severe magnetic field inhomogeneity without an unacceptable loss in SNR.

Keywords: NMR; Spectroscopy; High-resolution; Deconvolution; Imaging; Inhomogeneous fields

1. Introduction

The ability of NMR to provide valuable information about the chemical environment of the nucleus under investigation is largely dependent on the homogeneity of the magnetic field in which the experiment is performed. Typically, homogeneities of less than 1 ppm are required to achieve a frequency resolution such that chemical shifts for most nuclear species can be resolved. In some practical situations it is not feasible to provide a magnetic field of sufficient uniformity over the test region such that the desired spectral resolution can be achieved. For example in one-sided access (OSA) NMR, where a magnetic field is projected outside a surface so as to obtain an NMR signal from a material which is exterior to the apparatus, it is common for the magnetic field over the test region to range from 100 to 10,000 ppm [1]. In order to extract information about spectral properties, much narrower in frequency spread than the inhomogeneity induced spectral linewidth, it is necessary to provide other approaches to this problem.

Shimming is often used to significantly improve field homogeneity to an extent such that chemical shifts can be observed. In the case of one-sided access NMR the typical field inhomogeneities are much more severe than in laboratory based magnets. Furthermore, the design and implementation of shimming coils presents a problem because of the limited space available and also because of the high probability that the field inhomogeneity may contain higher order derivatives of the magnetic field that cannot be accessed by the shim field. Therefore, while B_0 shimming techniques may improve the inhomogeneous line broadening, this improvement is generally insufficient to resolve chemical shift information [2].

A number of novel approaches to the problem of extracting high-resolution NMR spectra from inhomogeneous fields have been proposed [2–7] each of which is, in a sense, a variant of the traditional shimming idea; however, instead

* Corresponding author. Fax: +64 6 350 5164.
E-mail address: Paul.Callaghan@vuw.ac.nz (P.T. Callaghan).

1090-7807/$ - see front matter © 2007 Elsevier Inc. All rights reserved.
doi:10.1016/j.jmr.2006.12.005

of using static shim fields, sometimes shim B_1 pulses are employed to match and cancel the effects of B_0 inhomogeneity. The method proposed in this paper is entirely different for no attempt is made to cancel the effects of the inhomogeneous fields. Instead these effects are removed during a robust data-processing step.

A component of our approach relies on the well-known method of reference deconvolution [8]. Information about the magnetic field inhomogeneity is obtained by acquiring a reference NMR signal from a sample whose spectrum is known precisely. In the case of proton NMR, that most relevant to one-sided access NMR, the reference sample would normally be water. Using this reference NMR signal, the signal obtained from an unknown sample can be deconvolved so as to remove that part of the spectral line-shape due to magnetic field inhomogeneity thus revealing the desired spectrum arising from the chemical shifts of the sample under investigation. Deconvolution in the spectral (frequency) domain is easily performed in the "Fourier" (time) domain by dividing the unknown sample time-domain signal by the known sample time-domain signal. Clearly such signal division makes for signal-to-noise ratio difficulties at longer times when the known sample signal has decayed to the level of the noise. However the reference signal may be acquired once using a very large number of acquisitions, optimising the available signal-to-noise ratio for this reference. The time taken for the known sample signal to decay is inversely related to the inhomogeneous line broadening and thus the deconvolution method breaks down when the inhomogeneous line-width is much larger than the spectral features to be resolved.

In our proposed method we take advantage of a feature of one-sided access NMR which makes deconvolution particularly effective, that is the fact that the characteristics of the inhomogeneous field region are the same for all samples of size larger than the sensitive volume of the apparatus, provided that the same magnet system is used and the same RF pulse excitation conditions are used, thus ensuring that the same sensitive volume is excited. This makes it possible to obtain the reference signal with arbitrarily high signal-to-noise ratio, by simply acquiring the reference signal data for a very long time. This reference signal, once acquired, can be stored and used for all subsequent deconvolutions.

The new element of the deconvolution part of our method relies on the fact that the line broadening arises from spatial inhomogeneity, i.e. the spatial variation of the magnetic field across the target region of the sample. Fig. 1 presents a schematic of our method. Effectively we use chemical shift imaging techniques to divide the sample volume (shown on the left in Fig. 1) into separate smaller pieces and acquire a set of sub-sample NMR signals from these sub-regions [9]. Because these regions are necessarily smaller than the total sensitive volume, their individual line broadenings are smaller than that for the spectrum corresponding to the entire target volume, although still too broad to resolve high-resolution frequency information such as chemical shift. This high-resolution information is obtained by performing deconvolution on each sub-sample. In order to deconvolve each sub-sample, we use separate reference signals obtained from identical sub-samples of the reference sample (depicted on the right in Fig. 1). The deconvolved sub-sample signals are then summed to

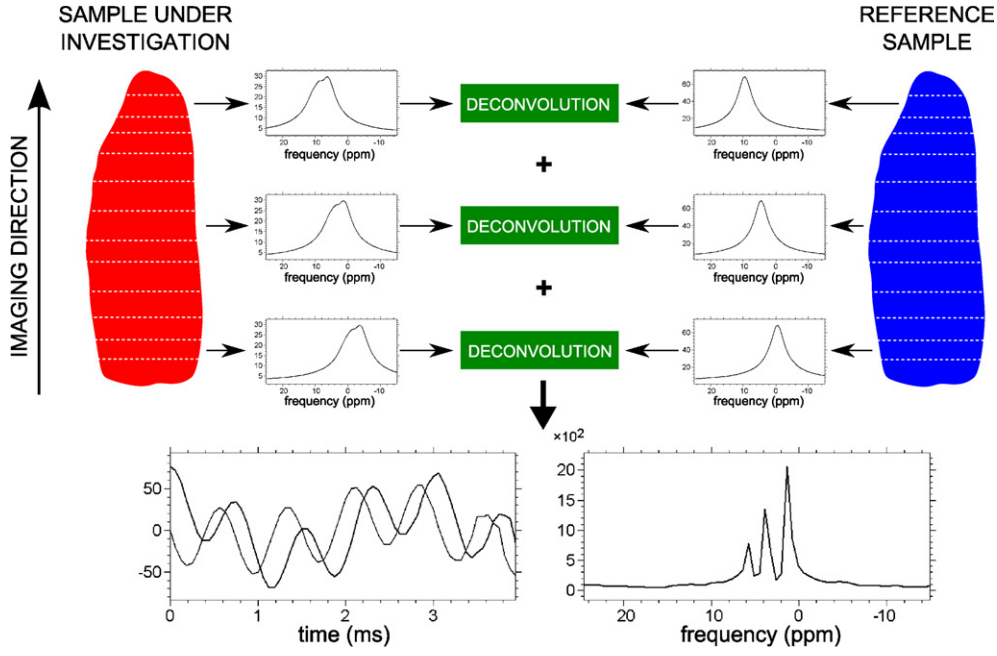

Fig. 1. A schematic of the imaged deconvolution process. On the left in the figure the target volume of the sample under investigation is divided into sub-regions in the direction of an imaging gradient. A spectrum is acquired from each sub-region of the sample, such that the line broadening in each is significantly less than the line broadening across the entire sensitive volume. The same process is applied to the reference sample, depicted on the right, and the resultant reference sample spectra are used to deconvolve each of the localised spectra of the sample under investigation. The resultant high-resolution deconvolved spectra are summed, in the time domain, to recover, in part, the SNR sacrificed by the subdivision of the target volume into sub-regions.

recover some of the signal-to-noise ratio (SNR) forfeited through the initial subdivision of the sample.

We have found that our method, which we call "imaged deconvolution", works even if a single uniform imaging gradient is used, despite a prevailing non-uniform inhomogeneous field. It is ideal, however, that the single gradient has its field varying most strongly along the direction in which the background inhomogeneous field varies most strongly. In one-sided access NMR this will typically be the direction normal to the surface of the magnet array. All that is necessary is to break the sample into sufficiently small regions of space so that the resolution in each such region is automatically improved to such an extent that deconvolution can be successfully applied to each sub-sample.

The process of using NMR imaging to compute separate NMR spectra from N sub-samples and then subsequently co-adding the spectra to produce a final total spectrum has a signal-to-noise ratio disadvantage of $N^{1/2}$ by comparison with simply acquiring the same total signal N times and co-adding each signal. However it has a signal-to-noise ratio advantage of $N^{1/2}$ compared with breaking the total NMR signal into N separate sub-sample signals, for example by selective excitation or line scanning.

Due to the $N^{1/2}$ SNR disadvantage of the imaging method, there is a "crossover regime" where imaged deconvolution becomes superior to simple deconvolution without imaging (raw deconvolution). We show herein that imaged deconvolution wins over raw deconvolution if it is necessary to reduce the inhomogeneous line-width by more than a factor of 7. This will almost always be the case in practical efforts to improve spectral resolution of NMR performed with an inhomogeneous field. Typical line-widths will at best be 100 ppm, and the typical desired resolution will be on the order of 1 ppm, sufficient to resolve water and oil (3.5 ppm) in the proton NMR spectrum.

When considering the method of imaged deconvolution, one obvious question is whether it might be possible to achieve high resolution spectroscopy by means of imaging alone, that is, by reducing the size of the voxels until the desired spectral resolution is achieved without the use of deconvolution. Such a methodology has been proposed by Sersa and Macura [10]. The disadvantage of this approach in the case of grossly inhomogeneous fields is that the spectral resolution is ultimately limited by that of the "poorest performing voxel". In other words, very high spatial resolution may be required, in three dimensions and with a very large number of voxels. Furthermore the route to high spectral resolution via imaging alone would require large and highly uniform gradients.

The method we propose is a compromise between the two approaches of pure deconvolution and pure spectroscopic imaging. Pure deconvolution, while easy to implement, does not work in the case of large line broadening, whereas pure spectroscopic imaging places impractical demands on both hardware and experiment time. Our method of imaged deconvolution finds the optimal compromise between these two methods so as to render the acquisition of high resolution spectra in grossly inhomogeneous fields possible.

2. Theory

Let $|\mathbf{B}(\mathbf{r})|$ be the magnitude of the inhomogeneous magnetic field in which the spins are immersed and using which the NMR signal is acquired. Let G be the amplitude of an additional applied magnetic field gradient pulse, applied in a phased-encoding manner, as shown in Fig. 2. For the purposes of mathematical demonstration we will assume that the background inhomogeneous field can be approximated by a single axis gradient, i.e. $G_{\mathrm{in}} = \frac{\partial|\mathbf{B}(\mathbf{r})|}{\partial x}$. In practice, this need not be so.

Suppose that the unknown sample (multi-line) spectrum $s(f)$ corresponds in the time domain to a free induction decay (FID) signal $S(t)$. Then the resultant spectrum in the presence of the magnetic field gradient is $s_{\mathrm{B}}(f) \otimes s(f)$ where $s_{\mathrm{B}}(f)$ is the line-broadening spectrum associated with the magnetic field inhomogeneity and $\otimes$ represents a convolution. The line broadening function $s_{\mathrm{B}}(f)$ may be expressed as the Fourier transform of its corresponding time domain response, $S_{\mathrm{B}}(t) = \int \mathrm{d}\mathbf{r}\rho(\mathbf{r}) \exp(\mathrm{i}\gamma|\mathbf{B}(\mathbf{r})|t)$ where $\rho(\mathbf{r})$ is a density function describing the number of spins at position $\mathbf{r}$. Using the convolution theorem of Fourier transforms, we can write the experimental time domain signal associated with the resultant spectrum, $s_{\mathrm{B}}(f) \otimes s(f)$, as a product of the time domain signals $S_{\mathrm{B}}(t)$ and $S(t)$: $S_{\mathrm{E}}(t) = S_{\mathrm{B}}(t)S(t) = \int \mathrm{d}\mathbf{r}\rho(\mathbf{r}) \exp(\mathrm{i}\gamma|\mathbf{B}(\mathbf{r})|t)S(t)$. In the method of deconvolution $S_{\mathrm{E}}(t)$ is divided by $S_{\mathrm{B}}(t)$ to obtain $S(t)$.

Let there be N phase-encoding gradient steps, so that we associate with each phase gradient pulse of amplitude G_{p} and duration t_{p} a "k-space" value $k = (2\pi)^{-1}\gamma G_{\mathrm{p}} t_{\mathrm{p}}$ where γ is the nuclear magnetogyric ratio. Let the random noise be given by $n^{\mathrm{R}}(t)$. For simplicity we shall treat the problem in 1-D of k-space and just write $B(x)$ instead of $|\mathbf{B}(\mathbf{r})|$. This simplification will serve our purpose of showing the crossover of benefit by comparison with raw deconvolution. The experimental signal, for one particular k-encode, is given by:

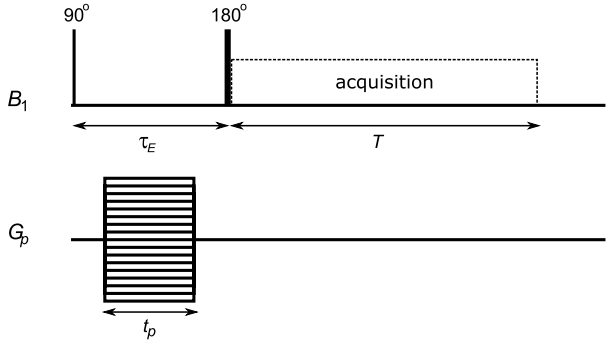

Fig. 2. The pulse sequence employed to acquire localised spectra from sub-regions of the sensitive volume, where TE, the echo time, is equal to $2 * \tau_{\mathrm{E}}$, T is the acquisition time and t_{p} is the phase encode gradient duration.

$$S_{\mathrm{E}}(k,t) = \int \rho(x)\exp(\mathrm{i}2\pi kx)\exp(\mathrm{i}\gamma B(x)t)\,\mathrm{d}x S(t) + n_k^{\mathrm{R}}(t), \quad (1)$$

where $\rho(x)$ is the nuclear spin density along the x-axis. Note that the noise is a function of time and is labelled by the k-value for which it is acquired.

In practice we sample a finite k-space and perform a discrete FT on the k-space data. Let the field of view (FOV) in the phase encode direction be $N\Delta x$ with the domain of x being $n\Delta x$ with n ranging from $-N/2$ to $N/2$ (in practice, with even N it is required to range from $-N/2+1$ to $N/2$ in order to make N intervals, but for simplicity of notation, we avoid this distinction). Thus the k-space domain is $m\Delta k$ where $\Delta k = 1/\mathrm{FOV} = 1/N\Delta x$ and m ranges from $-N/2$ to $N/2$. Hence

$$\begin{aligned} S_{\mathrm{E}}(k_m,t) &= \sum_{n=-N/2}^{N/2} \rho_n \exp(\mathrm{i}2\pi m\Delta k n\Delta x) \\ &\quad \times \frac{1}{\Delta x}\int_{(n-1)\Delta x}^{n\Delta x} \exp(\mathrm{i}\gamma B(x)t)\,\mathrm{d}x S(t) + n_m^{\mathrm{R}}(t) \\ &= \sum_{n=-N/2}^{N/2} \rho_n \exp(\mathrm{i}2\pi mn/N) \\ &\quad \times \frac{1}{\Delta x}\int_{(n-1)\Delta x}^{n\Delta x} \exp(\mathrm{i}\gamma B(x)t)\,\mathrm{d}x S(t) + n_m^{\mathrm{R}}(t). \end{aligned} \quad (2)$$

Note that ρ_n is the density contribution from the nth pixel, where $\sum_{n=-N/2}^{N/2}\rho_n = 1$ and for a reasonably uniform object, ρ_n:$1/N$.

Now we transform to the spatial domain using a discrete FT of the form $\sum_{m=-N/2}^{N/2}\exp(-\mathrm{i}2\pi mn/N)\cdots$. Note it is sometimes customary to preface this by $(1/N)$. So long as we are consistent in treating the signal and the noise the same, this pre-factor is immaterial. Hence, the spatial domain of FIDs is given by

$$\begin{aligned} S_{\mathrm{E}}(x_n,t) &= \sum_{m=-N/2}^{N/2}\sum_{n'=-N/2}^{N/2} \rho_{n'}\exp(-\mathrm{i}2\pi mn/N)\exp(\mathrm{i}2\pi mn'/N) \\ &\quad \times \frac{1}{\Delta x}\int_{(n'-1)\Delta x}^{n'\Delta x} \exp(\mathrm{i}\gamma B(x)t)\,\mathrm{d}x S(t) \\ &\quad + \sum_{m=-N/2}^{N/2} \exp(-\mathrm{i}2\pi mn/N) n_m^{\mathrm{R}}(t) \\ &= \sum_{n'=-N/2}^{N/2}\rho_{n'}\sum_{m=-N/2}^{N/2}\exp(\mathrm{i}2\pi m(n-n')/N) \\ &\quad \times \frac{1}{\Delta x}\int_{(n'-1)\Delta x}^{n'\Delta x} \exp(\mathrm{i}\gamma B(x)t)\,\mathrm{d}x S(t) \\ &\quad + \sum_{m=-N/2}^{N/2} \exp(-\mathrm{i}2\pi mn/N) n_m^{R}(t). \end{aligned} \quad (3)$$

Of course $\sum_{m=-N/2}^{N/2}\exp(\mathrm{i}2\pi m(n-n')/N) = 0$ unless $n = n'$, in which case the sum is N. Thus

$$\begin{aligned} S_{\mathrm{E}}(x_n,t) &= N\rho_n \frac{1}{\Delta x}\int_{(n-1)\Delta x}^{n\Delta x} \exp(\mathrm{i}\gamma B(x)t)\,\mathrm{d}x S(t) \\ &\quad + \sum_{m=-N/2}^{N/2} \exp(-\mathrm{i}2\pi mn/N) n_m^{\mathrm{R}}(t). \end{aligned} \quad (4)$$

Now $\sum_{m=-N/2}^{N/2}\exp(-\mathrm{i}2\pi mn/N)n_m^{\mathrm{R}}(t)$ is just a sum of N random noise trains each weighted by a changing m-dependent phase factor. Since the phase between different m noise trains is random anyway, this is equivalent to adding N incoherent noise functions. The result is $\sum_{m=-N/2}^{N/2}\exp(-\mathrm{i}2\pi mn/N)n_m^{\mathrm{R}}(t) = \sqrt{N}n_m^{\mathrm{R}}(t)$. Thus our final expression is

$$\begin{aligned} S_{\mathrm{E}}(x_n,t) &= N\rho_n \frac{1}{\Delta x}\int_{(n-1)\Delta x}^{n\Delta x} \exp(\mathrm{i}\gamma B(x)t)\,\mathrm{d}x S(t) + \sqrt{N}n_m^{\mathrm{R}}(t) \\ &= N\rho_n\left[\frac{1}{\Delta x}\int_{(n-1)\Delta x}^{n\Delta x}\exp(\mathrm{i}\gamma B(x)t)\,\mathrm{d}x\right]S(t) + \sqrt{N}n_m^{\mathrm{R}}(t). \end{aligned} \quad (5)$$

Note that the term in square brackets is a normalised envelope decay function, and is 1 at $t = 0$.

Deconvolution in the time domain involves dividing each experimental time domain signal $S_{\mathrm{E}}(x_n,t)$ by the equivalent reference signal $S_{\mathrm{Ref}}(x_n,t)$ acquired using the reference sample of very small intrinsic linewidth. Because the reference signal has a very small intrinsic linewidth its corresponding idealised time-domain signal decays very slowly with time, and to within a fixed phase shift (associated with the exact resonance frequency of the reference sample) we may write

$$S_{\mathrm{Ref}}(x_n,t) = N_{\mathrm{Ref}}N\rho_n^{\mathrm{Ref}}\left[\frac{1}{\Delta x}\int_{(n-1)\Delta x}^{n\Delta x}\exp(\mathrm{i}\gamma B(x)t)\,\mathrm{d}x\right]. \quad (6)$$

Note that the reference signal is acquired with many more signal averages (factor N_{Ref}) than the unknown sample signal. Consequently we omit the noise term for the reference signal since the reference signal-to-noise ratio may be made arbitrarily larger than that for the unknown sample. Clearly division of $S_{\mathrm{E}}(x_n,t)$ by $S_{\mathrm{Ref}}(x_n,t)$ yields the desired signal $S(t)$ along with an additional noise term which grows with increasing time as $\sqrt{N}n_m^{\mathrm{R}}(t)/[N_{\mathrm{Ref}}N\rho_n^{\mathrm{Ref}}\frac{1}{\Delta x}\int_{(n-1)\Delta x}^{n\Delta x}\exp(\mathrm{i}\gamma B(x)t)\,\mathrm{d}x]$. Obviously the division works perfectly on the signal part. It is on the noise that differences arise and through which limitations to the method arise. We may disregard the factor N_{Ref} henceforth.

Now we compare the imaging and raw deconvolution approaches for an equal total experimental time, involving N separate acquisitions. In the imaged deconvolution method, the deconvolved time domain signal is obtained by summing each separately deconvolved signal from every pixel, namely

$$S_{\mathrm{DC}}(t) = \sum_{n=-N/2}^{N/2} \left\{ S_{\mathrm{E}}(x_n, t) \Big/ \left[\frac{1}{\Delta x} \int_{(n-1)\Delta x}^{n\Delta x} \exp(\mathrm{i}\gamma B(x)t)\,\mathrm{d}x \right] \right\} \approx NS(t) + \sqrt{N} \sum_{n=-N/2}^{N/2} n_m^{\mathrm{R}}(t) \Big/ \left[\frac{1}{\Delta x} \int_{(n-1)\Delta x}^{n\Delta x} \exp(\mathrm{i}\gamma B(x)t)\,\mathrm{d}x \right]. \tag{7}$$

In the raw deconvolution method, the deconvolved time domain signal for summing N FIDs without imaging gradients is

$$S_{\mathrm{DC}}(t) = \sum_{n=-N/2}^{N/2} S_{\mathrm{E}}(t) \Big/ \left[\frac{1}{N\Delta x} \int_{-N\Delta x/2}^{N\Delta x/2} \exp(\mathrm{i}\gamma B(x)t)\,\mathrm{d}x \right] \approx NS(t) + \sqrt{N} n_m^{\mathrm{R}}(t) \Big/ \left[\frac{1}{N\Delta x} \int_{-N\Delta x/2}^{N\Delta x/2} \exp(\mathrm{i}\gamma B(x)t)\,\mathrm{d}x \right]. \tag{8}$$

Thus the relative performance comes down to a comparison of the noise functions:

$$\sqrt{N} \sum_{n=-N/2}^{N/2} n_m^R(t) \Big/ \left[\frac{1}{\Delta x} \int_{(n-1)\Delta x}^{n\Delta x} \exp(\mathrm{i}\gamma B(x)t)\,\mathrm{d}x \right] \tag{9}$$

and

$$\sqrt{N} n_m^{\mathrm{R}}(t) \Big/ \left[\frac{1}{N\Delta x} \int_{-N\Delta x/2}^{N\Delta x/2} \exp(\mathrm{i}\gamma B(x)t)\,\mathrm{d}x \right]. \tag{10}$$

We can easily estimate these, either by using exponential decays or sinc functions. Let us take the case of a constant local inhomogeneity gradient, G_{in}, for simplicity. In this case the integrals have very simple forms, i.e.

$$\left[\frac{1}{\Delta x} \int_{(n-1)\Delta x}^{n\Delta x} \exp(\mathrm{i}\gamma B(x)t)\,\mathrm{d}x \right] = \mathrm{sinc}(\gamma G_{in}\Delta x t/2)$$

and

$$\left[\frac{1}{N\Delta x} \int_{-N\Delta x/2}^{N\Delta x/2} \exp(\mathrm{i}\gamma B(x)t)\,\mathrm{d}x \right] = \mathrm{sinc}(\gamma G_{\mathrm{in}} N\Delta x t/2).$$

Note that the un-imaged FID case decays N times faster. The effect of these

$$\left[\frac{1}{\Delta x} \int_{(n-1)\Delta x}^{n\Delta x} \exp(\mathrm{i}\gamma B(x)t)\,\mathrm{d}x \right]^{-1}$$

functions is to "explode the noise" in the time domain. Clearly the comparison between the two cases is highly non-linear.

Finally we obtain the Fourier transform with respect to t to calculate the spectrum. Here we see what this does with the "exploding" time domain noise in each case. Instead of using sinc functions, we use exponential decays for mathematical tractability. For the N co-added FIDs, the decay function will be something like $\exp(-\gamma G_{\mathrm{in}} N\Delta x t)$ and for the N "imaged" pixel FIDs, the individual decay functions will be something like $\exp(-\gamma G_{\mathrm{in}}\Delta x t)$. The "explosion functions" are then nice and simple, i.e. $\exp(\gamma G_{\mathrm{in}} N\Delta x t)$ and $\exp(\gamma\ G_{\mathrm{in}}\Delta x t)$.

Using these integrals we can now make the comparison of the noises $\sqrt{N}\sum_{n=-N/2}^{N/2} n_m^{\mathrm{R}}(t)\exp(\gamma G_{\mathrm{in}}\Delta x t)$ and $\sqrt{N} n_m^{\mathrm{R}}(t)\exp(\gamma G_{\mathrm{in}} N\Delta x t)$. Let the total sampling time be T, so that the spectral resolution interval is $1/T$. The FT process will involve an integral over the noise functions with changing phase factors. Again, under an FT, the effect is as if the noise is integrated. To gain some idea of the order of magnitude of the noise, we need to find the integrals

$$\frac{1}{T}\int_0^T \exp(\gamma G_{\mathrm{in}} N\Delta x t)\,\mathrm{d}t$$

and

$$\frac{1}{T}\int_0^T \exp(\gamma G_{\mathrm{in}}\Delta x t)\,\mathrm{d}t,$$

i.e.

$$\frac{1}{\gamma G_{\mathrm{in}} N\Delta x T}\exp(\gamma G_{\mathrm{in}} N\Delta x T)$$

and

$$\frac{1}{\gamma G_{\mathrm{in}}\Delta x T}\exp(\gamma G_{\mathrm{in}}\Delta x T).$$

The frequency domain noise for the imaged deconvolution case is on the order of $N\frac{1}{\gamma G_{\mathrm{in}}\Delta x T}\exp(\gamma G_{\mathrm{in}}\Delta x T)\langle n^{\mathrm{R}}(t)^2\rangle^{1/2}$. The frequency domain noise for the raw deconvolution case is on the order of $\sqrt{N}\frac{1}{\gamma G_{\mathrm{in}} N\Delta x T}\exp(\gamma G_{\mathrm{in}} N\Delta x T)\langle n^{\mathrm{R}}(t)^2\rangle^{1/2}$.

Thus for summing each pixel to win in terms of a more favourable resultant SNR we require that $N\exp(\gamma G_{\mathrm{in}}\Delta x T) < N^{-1/2}\exp(\gamma G_{\mathrm{in}} N\Delta x T)$. Taking natural logs, this means:

$$\tfrac{3}{2}\log N < \gamma G_{\mathrm{in}}\Delta x(N-1)T. \tag{11}$$

Note $\gamma G_{\mathrm{in}}\Delta x(N-1)T$ is approximately the decay exponent gained by the full sample at the end of the time interval. In other words $\gamma G_{\mathrm{in}}\Delta x(N-1) \sim \gamma G_{\mathrm{in}}\mathrm{FOV}$, which is the raw linewidth. The left hand side of Eq. (11), for $N = 64$–128, will be on the order of 6–7. Thus the method of imaged deconvolution will win over raw deconvolution if there is a decay of more than e^{-7} across the sample. Of course, this will be determined by setting T and hence our spectral resolution, $1/T$. Therefore in the case of a target spectral resolution better than (1/7) of the inhomogeneous linewidth, the imaged deconvolution method will be more favourable. For cases of a target linewidth greater than (1/7) of the inhomogeneous linewidth, adding FIDs and performing raw deconvolution is more favourable. Thus for resolution improvements of an order of magnitude or more, the imaged deconvolution approach outperforms the raw deconvolution approach quite significantly.

3. Experimental

All experiments were performed on a Bruker Avance 400 spectrometer with a wide bore 9.4 T superconducting

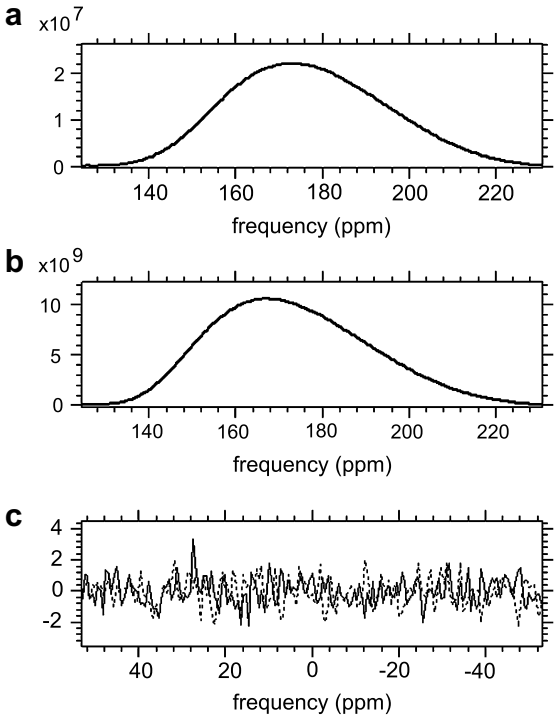

Fig. 3. Proton NMR spectra acquired of (a) ethanol and (b) water in the presence of a significant magnetic field inhomogeneity. The spectral linewidth, due to field inhomogeneity, is approximately 60 ppm. The water data was acquired with 8 times more averages than the ethanol data in order to achieve a very high SNR for the reference signal. The centre frequencies of the spectra in (a) and (b) are approximately 170 ppm. This is a consequence of the field offset generated by the inhomogeneity coil. This offset is removed by the deconvolution process. (c) The result of deconvolution of the ethanol spectrum in (a) by the reference water spectrum in (b) is dominated by noise due to the severity of the line-broadening. Note that the solid and dashed lines in (c) refer to the real and imaginary parts of the spectrum, respectively.

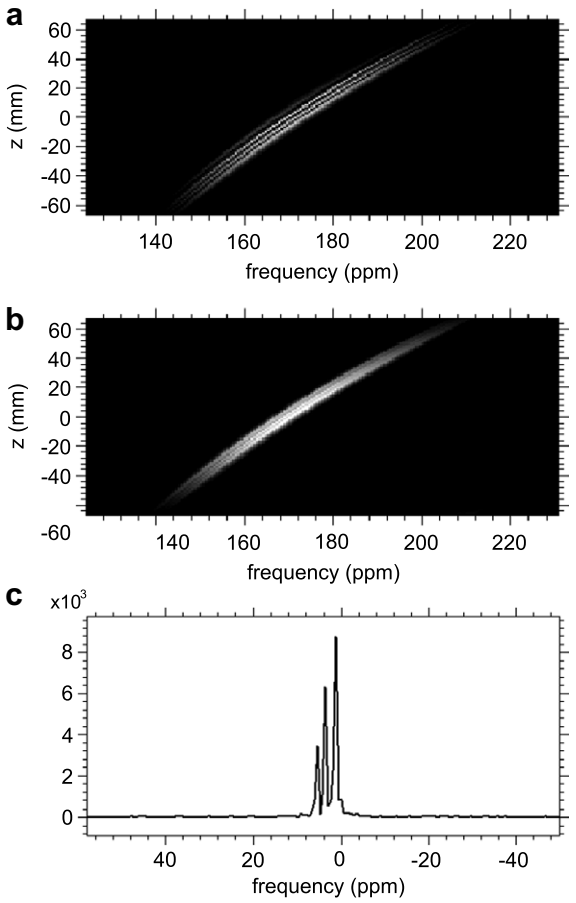

Fig. 4. The result of the imaged deconvolution method. Spatially resolved proton spectra acquired of (a) ethanol and (b) water. The water data is acquired with eight times more averages than the ethanol data in order to achieve a very high level of SNR for the reference signals. The spatially resolved spectra, like the spectra in Fig. 3(a) and (b) are offset by 170 ppm due to the field offset generated by the inhomogeneity coil. This offset is removed by the deconvolution process. (c) The high-resolution spectrum obtained by separately deconvolving the spatially resolved spectra of ethanol in (a) by those of water in (b) and summing the result. The ethanol spectrum is resolved to better than 1 ppm.

magnet. The water-cooled gradient set was capable of delivering 0.97 T/m at a maximum current of 40 A. The RF coil was a 10 mm diameter birdcage coil tuned to proton resonance (Bruker). The static magnetic field inhomogeneity was generated by placing a 220 turn, 38 mm diameter coil 58 mm from the centre of the sensitive region of the RF coil and passing 20 A through it. This coil generated a non-linear inhomogeneity of approximately 60 ppm across the sensitive region of the coil and also offset the static field by approximately 170 ppm. The samples used were a 5 mm NMR tube of distilled water and a 5 mm NMR tube of neat ethanol.

The proton NMR spectra in Fig. 3a and b were acquired using a standard spin-echo sequence with $TE = 8$ ms, $swh = 500$ kHz and $TR = 3$ s. Five hundred and twelve averages were acquired of the ethanol sample in a total acquisition time of 25 min. Four thousand ninety-six averages were acquired of the water sample in a total experiment time of 3 h and 20 min.

The spatially resolved proton spectra in Fig. 4a and b were acquired using the spin-echo chemical shift imaging experiment shown in Fig. 2. The experimental parameters were: $TE = 8$ ms, $swh = 500$ kHz, $G_{pmax} = 58.8$ mT/m, $t_p = 3.1$ ms, $N_p = 128$ and $TR = 3$ s. The water data set was acquired with 32 scans in 3 h and 20 min. The ethanol data set was acquired with 4 scans in 25 min.

All data processing was performed using the Prospa v2.1 software package (magritek Limited, Wellington, NZ).

4. Results/discussion

Fig. 3 presents NMR spectra acquired of (a) ethanol and (b) water in the presence of a severe non-linear magnetic field inhomogeneity. The inhomogeneity broadening in these spectra is approximately 60 ppm. Fig. 3c presents the result of deconvolving the ethanol spectrum in (a) with the water reference spectrum in (b). Note that the water spectrum is acquired with eight times more signal averages in order to provide a reference signal with high SNR. The

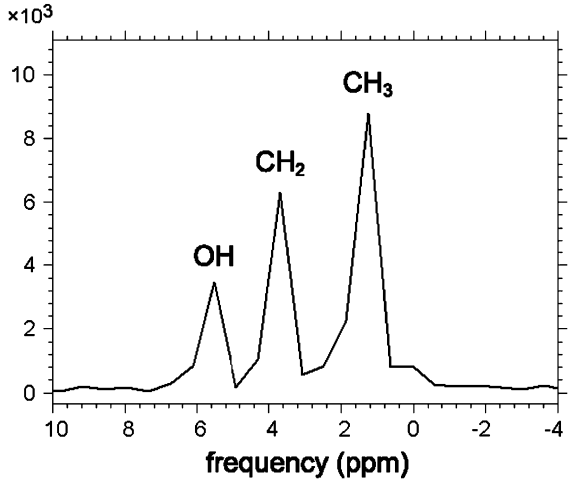

Fig. 5. The imaged deconvolution spectrum of neat ethanol from Fig. 4c zoomed in to reveal three peaks at 1.2 ppm (integral of 49.1%), 3.7 ppm (integral of 32.1%) and 5.5 ppm (integral of 18.8%). These peaks correspond to the three constituents of the ethanol sample: CH_3, CH_2 and OH, as indicated, and the relative chemical shifts are consistent with known literature values. The discrete nature of this spectrum is due to the finite number of data points (23 points over the displayed 14 ppm).

result of the deconvolution is dominated by noise because of the severity of the inhomogeneity line broadening.

Fig. 4 presents the results of the imaged deconvolution experiment. The total experiment time for imaged deconvolution was limited to that of the raw deconvolution experiment so as to allow for a valid comparison between the SNR performances of each method. The spatially resolved spectra for (a) ethanol and (b) water were acquired using the chemical shift imaging experiment presented in Fig. 2. Each spatially resolved ethanol spectrum was deconvolved in the time domain, using the corresponding water spectrum and the results were summed, in the time domain, and Fourier transformed to yield the high-resolution spectrum presented in Fig. 4c. The spectrum of neat ethanol is resolved to less than 1 ppm, with peaks at 1.2 ppm (integral of 49.1%), 3.7 ppm (integral of 32.1%) and 5.5 ppm (integral of 18.8%). These peaks can be assigned to the three constituents of ethanol: CH_3, CH_2 and OH, as shown in Fig. 5.

Comparison between Figs. 3 and 4 demonstrates the superior SNR performance of imaged deconvolution over raw deconvolution for obtaining high-resolution spectra in the presence of inhomogeneity line broadening significantly larger than the frequency spread of the spectral features to be resolved.

One of the significant benefits of this deconvolution based technique over a shimming-based technique, where a cancellation of the field homogeneity is sought either via shim B_0 fields or shim B_1 pulses, is that the field inhomogeneity need not be known with a high degree of precision. Beyond the characterisation obtained through the use of a reference signal, no a priori knowledge of the inhomogeneity is required. Furthermore there is no limit as to the types or orders of inhomogeneity which can be removed using this technique. The performance of the method is, however, improved if the imaging direction is chosen to coincide with the dimension in which the magnetic field inhomogeneity is the most pronounced. If the severity of the magnetic field inhomogeneity is significant in more than one orthogonal direction, it is possible to extend the method presented herein to contain up to three imaging dimensions.

Another advantage of imaged deconvolution is that no stipulations are made regarding the shape or regularity of the sub-regions into which the sample is divided during the imaging process. In order for the method to be successful, the volume of any given sub-region must necessarily be significantly smaller than the total target volume. However, the sub-regions need not be of the same size and shape. Therefore the method is insensitive to any non-linearity of the gradients or other non-ideal behaviours of the hardware as long as these non-ideal behaviours are the same for both the reference sample and the target sample.

It is anticipated that the application of imaged deconvolution to a one-sided access NMR system will face a few technical challenges. Even with the relatively small number of voxels needed for our method, the gradient strengths required to sub-divide the small sensitive region of a one-sided access type instruments will be significant. However, the current state of imaging gradient technology and the relative insensitivity of the methodology to moderate, reproducible non-ideal hardware behaviours suggests that the required gradient performance will not be prohibitive. The field stability of the magnet system is also a concern as the field of permanent magnet based systems varies significantly with temperature. In addition, the SNR performance and overall efficiency of the methodology will have to be optimised in order to make this methodology viable in practice.

The imaged deconvolution experiment presented in this paper employed a simple, non-optimised spin-echo chemical shift imaging sequence for the spatial localisation of the spectral information. However, the method is by no means limited to this type of acquisition scheme. It is anticipated that the efficiency of this technique will benefit greatly, not only from the optimisation of this imaging scheme but also from the incorporation of fast chemical shift imaging techniques [11,12]. In theory, the only constraints of the imaged deconvolution technique with regard to the imaging scheme are (a) that the reference signal be acquired with the same acquisition scheme as the target signal and (b) that each pixel is sufficiently small such that the inhomogeneous line broadening can successfully be removed via deconvolution.

5. Conclusions

We have demonstrated the ability of the imaged deconvolution method to extract high-resolution NMR spectra in the presence of a highly inhomogeneous static magnetic field. Furthermore, it has been demonstrated that in the case of inhomogeneous line broadening which is more than

an order of magnitude larger than the frequency spread of the spectral features to be resolved, the SNR performance of the imaged deconvolution approach is far superior to raw deconvolution. It is anticipated that with the optimisation of the spatial encoding step, through optimal parameter choices and/or the adoption of some of the available fast chemical shift imaging techniques, imaged deconvolution will provide a means of obtaining high-resolution NMR spectra in reasonable acquisition times, even in the presence of inhomogeneous line broadening orders of magnitude larger than the target spectral features.

Acknowledgments

The authors acknowledge grant support from the New Zealand Foundation for Research, Science and Technology and the Royal Society of New Zealand Marsden Fund and Centres of Research Excellence Fund. In addition, MEH would like to acknowledge the support of a Victoria University of Wellington post-graduate scholarship. We are grateful to Manu Pouajen-Blakiston and Alan Rennie for their help with the experimental setup.

References

[1] G. Eidmann, R. Savelsberg, P. Blumler, B. Blumich, The NMR-MOUSE: a mobile universal surface explorer, Journal of Magnetic Resonance Series A 122 (1996) 104–109.

[2] J. Perlo, F. Casanova, B. Blumich, Single-sided sensor for high-resolution NMR spectroscopy, Journal of Magnetic Resonance 180 (2006) 274–279.

[3] C.A. Meriles, D. Sakellariou, H. Heise, A.J. Moule, A. Pines, Approach to high-resolution ex-situ NMR spectroscopy, Science 293 (2001) 82–85.

[4] J. Perlo, V. Demas, F. Casanova, C.A. Meriles, J. Reimer, A. Pines, B. Blumich, Science 308 (2005) 1279.

[5] D. Topgaard, R.W. Martin, D. Sakellariou, C.A. Meriles, A. Pines, "Shim pulses" for NMR spectroscopy and imaging, Proceedings of the National Academy of Sciences of the United States of America 101 (2004) 17576–17581.

[6] Boaz Shapira, Lucio Frydman, Spatial encoding and acquisition of high-resolution NMR spectra in inhomogeneous field, Journal of the American Chemical Society 126 (2004) 7184–7185.

[7] Boaz Shapira, Lucio Frydman, Spatially encoded pulse sequences for the acquisition of high-resolution NMR spectra in inhomogeneous fields, Journal of Magnetic Resonance 182 (2006) 12–21.

[8] K.R. Metz, M.M. Lam, A.G. Webb, Reference deconvolution: a simple and effective method for resolution enhancement in nuclear magnetic-resonance spectroscopy, Concepts in Magnetic Resonance 12 (2000) 21–42.

[9] T.R. Brown, B.M. Kincaid, K. Ugurbil, NMR chemical-shift imaging in 3 dimensions, Proceedings of the National Academy of Science of the United States of America—Biological Sciences 79 (1982) 3523–3526.

[10] I. Sersa, S. Macura, Improvement of spectral resolution by spectroscopic imaging, Applied Magnetic Resonance 27 (2004) 259–266.

[11] R. Pohmann, M. VonKienlin, A. Haase, Theoretical evaluation and comparison of fast chemical shift imaging methods, Journal of Magnetic Resonance 129 (1997) 145–160.

[12] P. Mansfield, Spatial mapping of chemical-shift in NMR, Magnetic Resonance in Medicine 1 (1984) 370–386.